$K^0_S K^-$ Decay of A_2^- Produced by 20.3-GeV/c π^- on Hydrogen*

K. J. Foley, W. A. Love, S. Ozaki, E. D. Platner, A. C. Saulys, and E. H. Willen
Brookhaven National Laboratory, Upton, New York 11973

and

S. J. Lindenbaum
Brookhaven National Laboratory, Upton, New York 11973
and City College of the City University of New York, New York, New York 10031
(Received 30 March 1972)

We present the results of an analysis of data for the reaction $\pi^- p \to K^0_S K^- p$ at 20.3-GeV/c incident π momentum. We find that the $K^0 K^-$ effective-mass spectrum shows a single peak in the A_2 region which is well fitted by a Breit-Wigner shape. The data in the A_2-peak region are inconsistent with the split-A_2 shape reported earlier. The distribution in t of the A_2 events shows a forward dip followed by an exponential falloff. The A_2 decay angular distribution is well fitted by a single resonance with quantum numbers $J^P = 2^+$. The results of an analysis of the density-matrix elements for this reaction are given.

I. INTRODUCTION

We have studied the reaction $\pi^- p \to K^0_S K^- p$ at 20.3-GeV/c incident momentum using the BNL double-vee magnetic spectrometer to measure the angles and the momenta of the K^- and the two charged pions from the decay of the K^0_S. The purpose of the experiment was to study the production and decay of $I = 1$ boson resonances decaying via the $K\bar{K}$ mode. The region of the A_2 meson ($\sim$ 1300 MeV) was of particular interest because of the apparent disagreement in the shape of the A_2 mass spectrum in several earlier experiments.[1-3] The results of an LBL bubble-chamber experiment[1] using a 7-GeV/c π^+ beam showed a simple Breit-Wigner shape with sufficient statistical precision to rule out the shape seen in the CERN missing-mass spectrometer data[2]: The latter data, obtained with π^- in the momentum region 2.6–7 GeV/c, showed a deeply split peak. There were also several other experiments[3] which seemed to indicate a split peak, but these had less statistical significance.

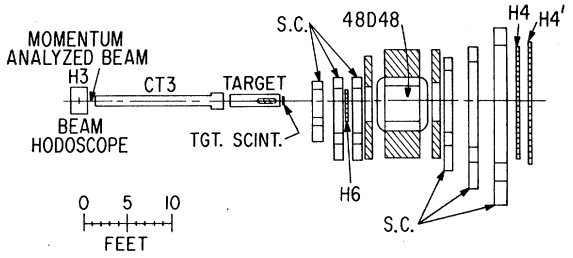

FIG. 1. The forward arm of the double-vee magnetic spectrometer used in this experiment. The symbols S.C. stand for spark chamber, H for scintillation counter hodoscope, and CT3 for threshold Čerenkov counter.

Earlier measurements[4] had shown that unlike the $p\pi$ channel, the $K^0_S K^-$ channel had very little nonresonant background. In addition, because of the good mass resolution obtained in this experiment, it was apparent that we could make a definitive statement on the A_2 shape even though the cross section in this channel is only about 2 μb at 20.3 GeV/c. Another feature of the low background is that precise determination of the A_2 spin density matrix is possible. The $K^0_S K^-$ mass spectrum from this experiment was published earlier.[5]

II. EXPERIMENTAL ARRANGEMENT AND PROCEDURE

The beam used for this experiment was an unseparated secondary negative beam produced at 0° by the slow extracted beam at the Brookhaven AGS. The momentum was 20.3 GeV/c. Two scintillation-counter hodoscopes were used to measure the angle of incidence at the hydrogen target to ±0.2 mrad (rms), while a third hodoscope upstream of a set of three bending magnets (8.7° total bend) permitted the incident momentum to be determined to ±0.2%. Threshold Čerenkov counters were used to select pions in the incident beam. We used approximately 40 000 incident beam particles per pulse, representing one third of the particle flux through the spark chambers, with a typical flat-top spill length of 300 msec.

The detection apparatus is shown in Fig. 1. It is the forward arm of the BNL double-vee spectrometer, which will be described in detail elsewhere.[6] Briefly, it is a high-resolution magnetic spectrometer using low-mass, aluminum wire spark chambers with magnetostrictive readout in front of and behind a 48D48 bending magnet (48 in.

wide by 48 in. long by 18 in. high, with 16.7-kG central field). The size of the active area of the spark chambers varied from 1 ft by 3 ft for the smallest chamber to 4 ft by 13 ft for the largest. All but two of the spark chamber modules (S.C.) shown in Fig. 1 consisted of two gaps of vertical wires measuring the x coordinate, two gaps of horizontal wires measuring the y coordinate, and one of "w" wires at 45° to x and y. The first module contained an extra set of x and y gaps, and the last module contained no w gap. The wire planes forming each gap contained parallel wires which increased the multiparticle efficiency of the system. Each wire plane was read out and the two readings averaged to give the position of the spark in the gap. This technique improves the position resolution of the chambers. Up to eight sparks could be encoded for each readout. In order to minimize biases in the apparatus acceptance, the beam area of the chambers was not deadened. The angular resolution varied from 0.4 mrad at 4 GeV/c to 0.15 mrad at 20 GeV/c. The momentum resolution varied from 0.25% at 4 GeV/c to 0.6% at 20 GeV/c. The liquid-hydrogen target had a cylindrical cell 2 ft long and 4 in. in diameter with 0.0075-in.-thick Mylar walls capped with 0.005-in.-thick Mylar domes. This cell was placed in a vacuum box with an incident beam port and 0.014-in.-thick Mylar windows in the forward direction and on the sides. Forty layers of aluminized Mylar superinsulation, total thickness 0.010 in., were used to insulate the cell.

The basic topology selected by the triggering system consisted of one charged particle and one neutral particle leaving the target, with the neutral particle decaying into two charged particles downstream of the target. Selection of this topology was achieved as follows:

(1) Pulse-height discrimination on a scintillation counter just downstream of the target was used to ensure that one and only one charged particle emerged from the target in the forward direction.

(2) The scintillation-counter hodoscope H6 was used to demand three or more particles 100 in. downstream of the target.

(3) Hodoscopes H4 and H4′ were set to require a total of three particles, with two in a "negative-particle" region and one in a "positive-particle" region. There is some overlap in the regions illuminated by positive and negative particles; a Monte Carlo study was used to define "negative-particle" and "positive-particle" regions. The trigger regions were larger than defined by the Monte Carlo study in order to avoid biases.

The resultant trigger rate was one trigger for 5000 incident beam particles.

In addition to the A_2 trigger, we triggered on two types of monitor events, each gated to give one event per pulse. One type selected the incident beam and was used to monitor the beam momentum and single-track-chamber efficiencies. The other trigger selected $\pi^+\pi^-\pi^-(\tau)$ decays of negative kaons in the beam in order to monitor a well-defined process with topology similar to the A_2 events.

The data were recorded on magnetic tape and transmitted in parallel to the PDP-10 computer of the BNL On-Line Data Facility. The computer did complete on-line analysis of about 10% of the events in order to give continuous information on spectrometer performance for real events, K^0 mass resolution, K^-K^0 mass spectrum, recoil mass spectrum, etc. In addition, the computer monitored the output of a fast-cycling DVM (16 readings per AGS pulse) which stepped sequentially through the various magnet shunt voltages, magnet Hall voltages and currents, high-voltage supply outputs, etc. The computer was programmed to type out a warning when any reading deviated from the set value by more than preset tolerance (typically 1% for quadrupole magnets and 0.1% for the dipole magnets).

III. DATA ANALYSIS

A. Pattern Recognition

The off-line analysis was performed on the BNL CDC 6600 computers. The major computing task was the pattern recognition problem of combining the spark coordinates into track segments. The technique used was to treat each two-dimensional "view" of the event separately and look for straight

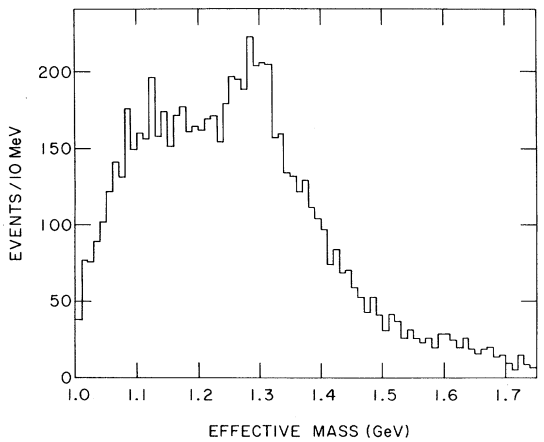

FIG. 2. The effective-mass spectrum for all events analyzed on the basis of the K^0K^- hypothesis.

line segments containing at least four sparks. The "X-view" and "Y-view" tracks thus found were combined into three-dimensional tracks by checking which combinations coincided with the sparks observed in the w planes (oriented at 45° to the x and y directions); then the track segments were connected through the magnet. A momentum was calculated for each track using a polynomial representation of the magnetic-field-length integral as a function of the incident angle, position, and approximate momentum of the track. (The approximate momentum was calculated assuming a uniform field.) Tracks which did not intersect triggered counters in the H4 hodoscope were so marked and ignored. Among the remaining tracks, three-dimensional vertices were sought downstream of the target counter. If the event fitted the topology of one negative prong plus a neutral vee in the mass region 0.485–0.510 GeV coming from a common point in the target, the momenta and positions of the tracks were written on a data-summary tape. This criterion was met by 0.5% of the triggers. Subsequent analysis was performed with the data-summary tape.

B. Kinematic Analysis

Since most of the computer analysis time went into pattern recognition, the use of the summary tape proved to be a great convenience. Starting with momenta and angles, all the events on the tape could be reanalyzed with any kinematic hypothesis in a very short period of time.

Since the decay products were not identified in the spectrometer, effective masses for both the K^0K^- and $K^0\pi^-$ hypotheses were calculated for each event. The effective-mass distribution for the K^0K^- hypothesis is shown in Fig. 2. No correction has been applied for the acceptance of the apparatus. A bump on top of a rather large background can be seen in the region of 1.3 GeV. The effective-mass plot for the $K^0\pi^-$ hypothesis for the same events is shown in Fig. 3. There is clear evidence of $K^*(890)$ production. The missing-mass spectrum of the events for the K^0K^- hypothesis is shown in Fig. 4. Events with a missing mass greater than 1.7 GeV are not shown. There is a clear peak at the proton mass with a full width at half maximum (FWHM) of ~140 MeV. We selected

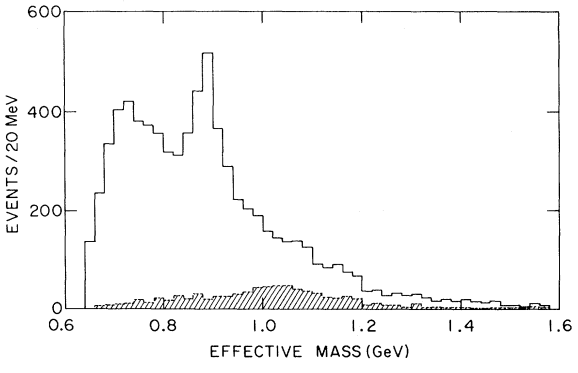

FIG. 3. The effective-mass spectrum for all events analyzed on the basis of the $K^0\pi^-$ hypothesis. There is a distinct peak at the mass of the $K^*(890)$. The shaded histogram is an effective-mass plot of those events identified as K^0K^- by cutting on the proton recoil, and then reanalyzed as $K^0\pi^-$.

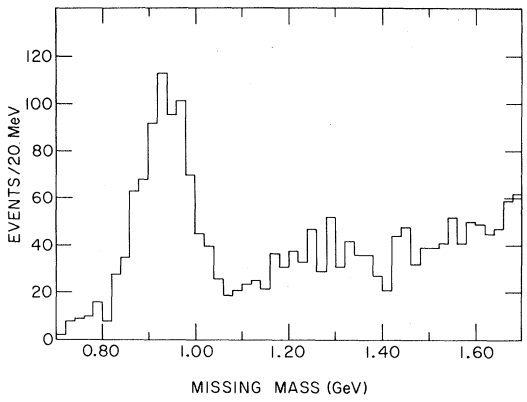

FIG. 4. The missing-mass spectrum for all events analyzed on the K^0K^- hypothesis. The events around the proton mass can only recoil from K^0K^-, and hence a strong discrimination is possible against $K^0\pi^-$.

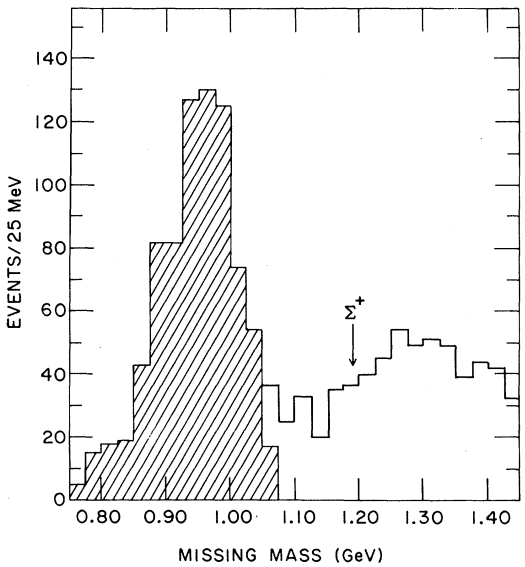

FIG. 5. The missing-mass spectrum for all events analyzed on the $K^0\pi^-$ hypothesis. The shaded part of the histogram corresponds to the final sample of K^0K^- events selected on the basis of the recoil proton mass.

the events with a missing mass in the region of 0.76–1.06 GeV. This sample represented ~0.05% of our triggers. From our missing-mass spectrum, we estimate that the background with recoil particles other than protons is less than ~5%.

The missing mass calculated on the basis of the $K^0\pi^-$ hypothesis is shown in Fig. 5. Clearly, there is no peak due to Σ^+ production. The final sample of K^0K^- events selected on the basis of the recoil proton mass (Fig. 4) is shown as a shaded histogram in Fig. 5. There is a negligible amount of background of $K^0\pi^-$ events in our K^0K^- data, since strangeness conservation would require a recoil mass at least as large as that of the Σ^+. We have also plotted the "$K\pi$" effective mass for the final data as the shaded histogram in Fig. 3. A smooth spectrum with no structure is obtained.

One further possible source of background, which could be troublesome in extracting decay correlations, is kinematic reflection from Y^* production in the reaction

$$\pi^- p \to K^0 Y^* \searrow K^- p.$$

We have calculated the missing mass from the K^0 for our events. This spectrum is shown in Fig. 6; there is no obvious structure and the spectrum is generally concentrated at mass higher than that of known Y^*'s. Thus, unlike measurements at low momentum, we expect negligible contamination from reflected Y^*'s.

IV. RESULTS

A. A_2 Mass Resolution

The A_2 effective-mass resolution was determined by the accuracy of measurement of the

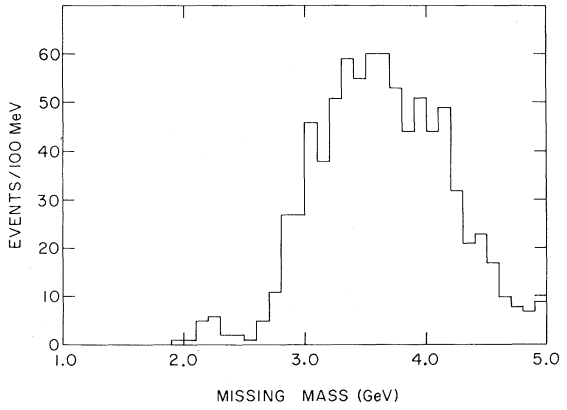

FIG. 6. The missing-mass spectrum from the K^0 for all K^0K^-p events. This figure shows that at this high momentum the experiment is not contaminated by Y^* production.

angles and momenta of its decay products. The largest contribution was the angular resolution of the spectrometer, which contributed approximately 50% to the square of the A_2 mass resolution. The momentum resolution contributed approximately 20%. The multiple scattering of the K^- in the hydrogen target and target counter contributed approximately 30%; all the accepted events had the K^0 decay point downstream of the target counter.

The angular resolution of the spectrometer was measured by sending beam particles at several momenta through the apparatus with the 48D48 magnet off and comparing the angles upstream and downstream of the magnet. The momentum resolution was obtained by sending beam particles through the apparatus at several momenta with the magnet on and comparing the momentum as measured by the beam spectrometer with that from the spark-chamber spectrometer.

Using these measurements, the calculated K^0 mass resolution agreed with the measured value of 2.7 ± 0.2 MeV for our A_2 events [see Table I and Fig. 7(a)]. In this experiment, the K^0 momentum spectrum from the A_2 decay varied over the range 4–17 GeV/c, peaking at 14.5 GeV/c. By including the contribution of the multiple scattering of the material upstream of our target counter, the calculation agreed with the measured resolution of 4.2 ± 0.2 MeV of the τ decays upstream of the hydrogen target, which were collected along with our A_2 data [Table I and Fig. 7(b)]. The major contribution to this last number is the multiple scattering in the hydrogen target of all three decay particles.

Having obtained agreement between measured and calculated values for the K^0 and K^- mass resolutions, we used the same angular and momentum resolutions to predict a value for the A_2 mass resolution of 3.5 ± 0.4 MeV. This calculation was done in two ways. One way was to fold the contributions due to multiple scattering, angular, and momentum resolutions. The other way was to take each observed A_2 event and, using a Monte Carlo technique, change the values of the angles and momenta of the three decay particles at random, consistent with our measured angular and momentum resolutions, and then recalculate the

TABLE I. The A_2^-, K^0, and K^- effective-mass resolution in this experiment.

Reaction	Particle	Measured σ (MeV)	Calculated σ (MeV)
$\pi^- p \to A_2^- p$	A_2^-	···	3.5 ± 0.4
$K_S^0 \to \pi^+\pi^-$	K^0	2.7 ± 0.2	2.8 ± 0.2
$K^- \to \pi^+\pi^-\pi^-$	K^-	4.2 ± 0.2	4.1 ± 0.2

A_2 effective mass. The width of this mass-difference distribution was consistent with that obtained by calculating the A_2 effective-mass resolution directly from the angular and momentum resolutions.

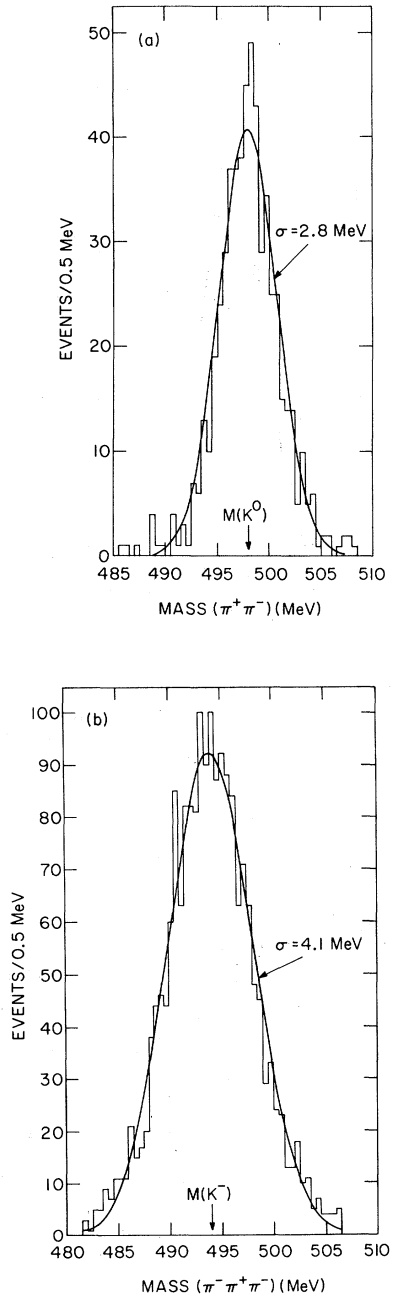

FIG. 7. (a) The reconstructed mass of K_S^0 decaying into 2π in this reaction. (b) τ decays (K^- decaying into 3π) in the beam recorded during the A_2 data runs. The curves are not fitted curves, but rather the values obtained from the Monte Carlo study (see text). The mass scale is uncertain by ≈0.5 MeV.

B. Apparatus Acceptance

The acceptance of the apparatus was evaluated by a Monte Carlo program which generated events for a range of values of the four kinematic variables t', m, $\cos\theta$, and φ, where t ($t'=t-t_{\min}$) is the negative of the four-momentum transfer squared for this reaction and θ and φ are the decay angles of the A_2 (defined in the Gottfried-Jackson frame[7]). The acceptances in this four-dimensional space were then used to perform the necessary normalization for maximum-likelihood fits to the mass spectrum, t dependence, and decay angular dependence of the data. The mass acceptance obtained by integrating the observed distributions in t', θ, and φ varies smoothly from 7.5% at a mass of 1.2 GeV to 4% at a mass of 1.4 GeV. Of the generated events, 55% were elim-

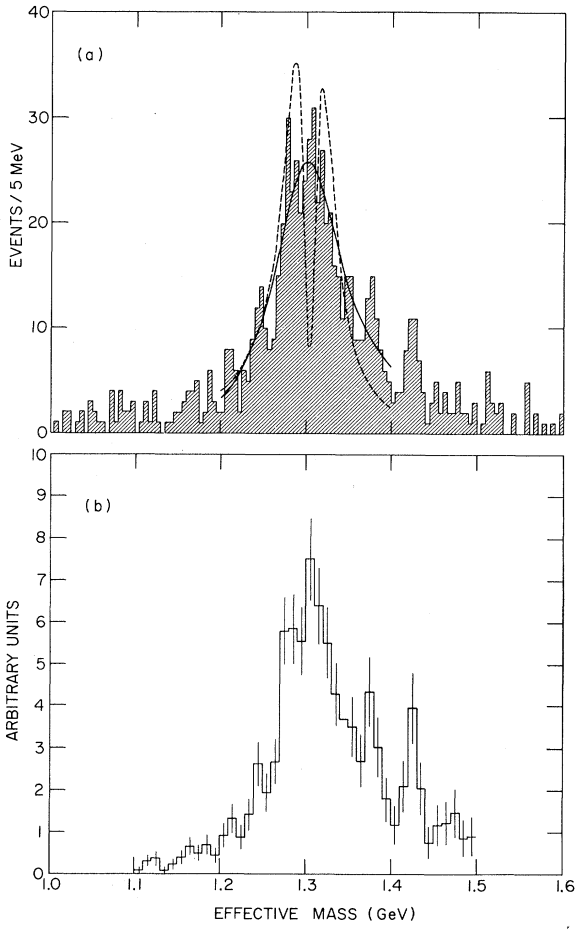

FIG. 8. The K^0K^- effective-mass spectrum for those events having a proton recoil; (a) uncorrected for acceptance, and (b) corrected for the acceptance of our apparatus. The A_2 signal at 1.3 GeV is produced with very little background. The curves are explained in the text. The mass scale is uncertain by ≈1 MeV.

inated by the target counter because the K^0 decayed in the hydrogen target.

C. Mass Spectrum

The distribution of K^0K^- effective mass is shown in Fig. 8. Figure 8(a) shows the data uncorrected for apparatus acceptance. There are 721 events in this spectrum. Figure 8(b) shows the mass spectrum in the range 1.1–1.5 GeV corrected for the apparatus acceptance.

There is no statistically significant structure in the peak centered at 1.3 GeV. We have fitted the data with the Breit-Wigner form expected for a D-wave resonance[8]:

$$\frac{mm_0\Gamma(m)}{(m^2-m_0^2)^2+[m_0\Gamma(m)]^2},$$

where

$$\Gamma(m)=\Gamma_0\left(\frac{q}{q_0}\right)^5\frac{\rho(q)}{\rho(q_0)},$$

$q_0=q(m_0)$, and q is the momentum of the K's in the A_2 rest frame. $\rho(q)$ is expected to be a slowly varying correction chiefly for angular momentum barrier effects. We have used

$$\rho(q)=(9+3R^2q^2+R^4q^4)^{-1},$$

where R is fitted as a free parameter.[9] The results of the maximum-likelihood fit[10] are $m_0=1.313\pm0.004$ GeV, $\Gamma_0=0.113\pm0.019$ GeV, $R^2=10\pm14$ GeV^{-2}, and $\chi^2=37.1$ for 36 degrees of freedom (d.f.), an excellent fit. This fit, modified by the acceptance, is shown as the solid line in Fig. 8(a). No background term was necessary in the fit.[11] Note that due to the distortion caused by $\Gamma(m)$, this functional form has a peak at 1304 MeV and has a full width at half maximum of 104 MeV.

A good fit is also obtained using the simple S-wave Breit-Wigner form

$$\frac{\Gamma/2}{(m-m_0)^2+(\Gamma/2)^2}.$$

$m_0=1.312\pm0.003$ GeV, $\Gamma=0.096\pm0.008$ GeV, and $\chi^2=45.7$ for 37 degrees of freedom. The stated errors are statistical only. The mass scale error is estimated to be approximately 1 MeV. The fit parameters are sensitive to uncertainties in the Monte Carlo parameters, however, and the estimated errors due to this effect are ±2 MeV on m_0 and ±1 MeV on the S-wave Γ. The D-wave Γ_0 is strongly correlated with the D-wave R parameter and slight changes in the shape of the mass acceptance produce large tradeoffs between these two parameters. Estimates of the acceptance error limits are ±6 MeV on Γ_0 with a correlated ∓9 GeV^{-2} on R_2^2.

No acceptable fit is possible with the dipole mass shape used for the CERN missing-mass data:

$$\left[\frac{(m-m_0)\Gamma}{(m-m_0)^2+(\Gamma/2)^2}\right]^2.$$

Using 4 MeV for the mass resolution, the best fit ($m_0=1.303$ GeV, $\Gamma=29$ MeV), within 5 MeV of the CERN parameters, is shown, modified for acceptance, as a dashed line on Fig. 8(a). The value of χ^2 (177 for 40 data points) corresponds to a 10-standard-deviation rejection. Searching the region $1.26<m_0<1.34$ GeV, $0.02<\Gamma<0.04$ GeV, we found no χ^2 better than 135, still nearly 8 standard deviations.

Another parametrization tried was the sum of two Breit-Wigner shapes. The best fit was obtained with most of the events in one peak centered near 1.30 GeV and about 8% of the events in a second peak centered near 1.38 GeV. Forcing the two Breit-Wigner shapes to have equal amplitudes gives a fit with the peaks superimposed on each other. From this we conclude that two incoherent Breit-Wigner shapes do not characterize the data.

Figure 9 shows the spectrum of K^0K^- effective mass for events with squared momentum transfer $|t'|>0.2$ (GeV/c)^2. We have examined the data over this t range using the parameters given for the fits shown in Fig. 8 with the results shown in Fig. 9. The statistics are not really adequate in this case (198 events in the range 1.2–1.4 GeV), but the single Breit-Wigner shape is still preferred, having a χ^2 of 38 (probability of ≈55%) versus a χ^2 of 61 (probability of ≈3%) for the double pole.

D. Differential Cross Section

The differential cross section $d\sigma/dt$ for the K^0K^- decay channel of the A_2^- is given in Table II

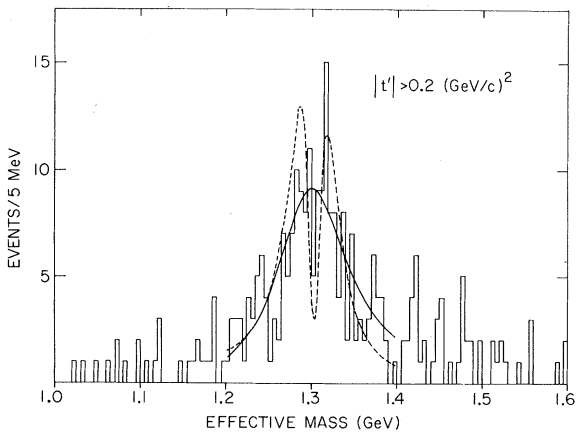

FIG. 9. The K^0K^- mass spectrum for those events of Fig. 8(a) with $|t'|$ greater than 0.2 (GeV/c)^2. The curves are the fits of Fig. 8(a) normalized to this data.

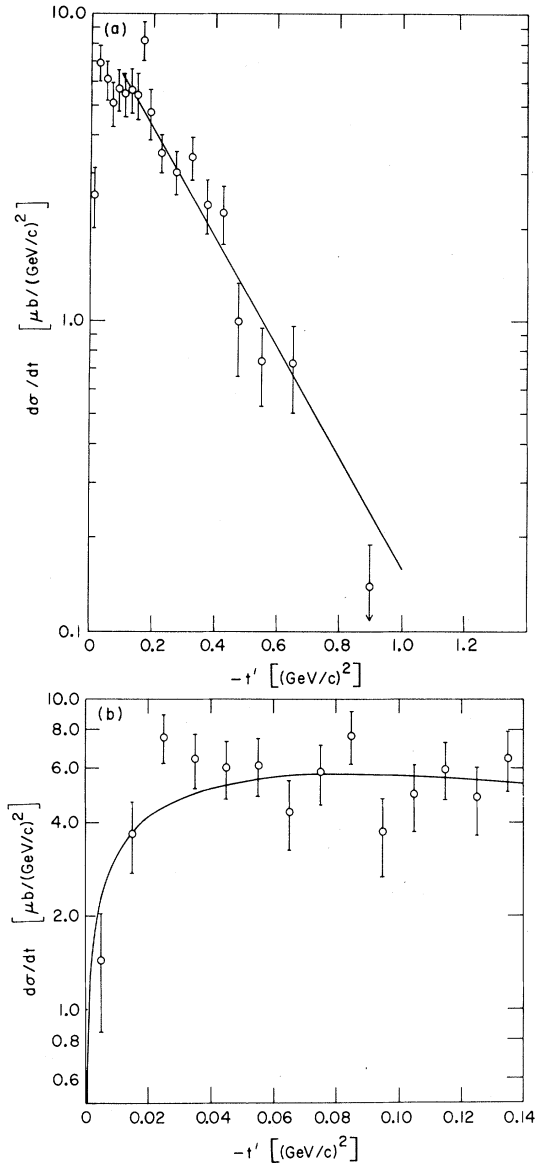

FIG. 10 (a) The t' distribution of events in the A_2 mass spectrum. The solid line is a fit of the form $e^{bt'}$ over the t' range $0.1 \leq |t'| \leq 1.0$ (GeV/c)^2. (b) The small-$|t'|$ region plotted in t' bins of 0.01 (GeV/c)^2. The dip in the forward direction is clearly evident in this plot. The solid line is a fit of the form $(-t')^a e^{bt'}$. We estimate a systematic scale uncertainty of ≈30% in the cross section in both (a) and (b).

TABLE II. The differential cross section for the reaction $\pi^- p \to A_2^- p$, with $A_2^- \to K^0 K^-$. The errors are statistical only. We estimate a systematic scale uncertainty of ±30% in the cross section.

t' [(GeV/c)^2]	$d\sigma/dt$ [μb/(GeV/c)^2]
0 to −0.02	2.55 ± 0.56
−0.02 to −0.04	6.93 ± 0.93
−0.04 to −0.06	6.09 ± 0.90
−0.06 to −0.08	5.10 ± 0.84
−0.08 to −0.10	5.67 ± 0.90
−0.10 to −0.12	5.47 ± 0.90
−0.12 to −0.14	5.63 ± 0.93
−0.14 to −0.16	5.42 ± 0.93
−0.16 to −0.18	8.23 ± 1.16
−0.18 to −0.20	4.76 ± 0.90
−0.20 to −0.25	3.50 ± 0.50
−0.25 to −0.30	3.04 ± 0.49
−0.30 to −0.35	3.39 ± 0.54
−0.35 to −0.40	2.37 ± 0.47
−0.40 to −0.45	2.24 ± 0.48
−0.45 to −0.50	0.99 ± 0.33
−0.50 to −0.60	0.74 ± 0.21
−0.60 to −0.70	0.73 ± 0.23
−0.70 to −1.1	0.14 ± 0.05

and shown in Fig. 10. The cross sections are corrected for the unseen K^0 branching fraction as well as for the fraction of the Breit-Wigner area outside our mass interval. The variation in acceptance is a smooth function of t. The errors given are statistical only. We estimate the systematic scale uncertainty in the cross section to be ≈30%.

The cross section shows a sharp forward dip near four-momentum transfer $t = t_{\min}$ and an exponential fall approximately as $e^{4t'}$ for $|t'|$ larger than 0.1 (GeV/c)^2. A maximum-likelihood fit to the form $(-t')^a e^{bt'}$ for the A_2 mass region 1.2–1.4 GeV gives values for the parameters $a = 0.48 \pm 0.08$ (GeV/c)$^{-2}$ and $b = 5.7 \pm 0.5$ (GeV/c)$^{-2}$. A maximum-likelihood fit to the form $e^{bt'}$ for the region $0.1 \leq |t'| \leq 1.0$ (GeV/c)^2, over the same A_2 mass range, gives a value for the parameter $b = 4.1 \pm 0.4$ (GeV/c)$^{-2}$. The errors given on the parameters are statistical only.

E. Spin Density Matrix

The normalized angular distribution of a spin-2^+ meson decaying to two pseudoscalar mesons is, in general,[8]

$$A(\theta,\phi) = \frac{15}{16\pi}\left[3\rho_{00}(\cos^2\theta - \tfrac{1}{3})^2 + 4\sin^2\theta\cos^2\theta(\rho_{11} - \rho_{1\,-1}\cos 2\phi) + \sin^4\theta(\rho_{22} - \rho_{2\,-2}\cos 4\phi)\right.$$
$$- 4\sqrt{6}\ \mathrm{Re}\rho_{10}(\cos^2\theta - \tfrac{1}{3})\cos\theta\sin\theta\cos\phi - 2\sqrt{6}\ \mathrm{Re}\rho_{20}(\cos^2\theta - \tfrac{1}{3})\sin^2\theta\cos 2\phi$$
$$\left. - 4\sin^3\theta\cos\theta(\mathrm{Re}\rho_{21}\cos\phi - \mathrm{Re}\rho_{2\,-1}\cos 3\phi)\right]. \qquad (1)$$

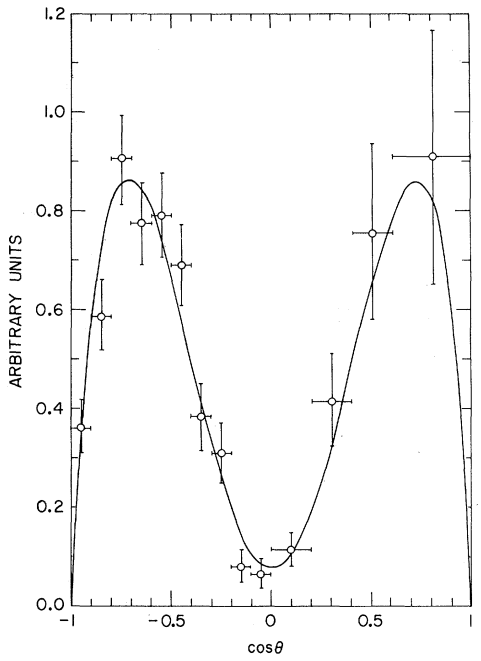

FIG. 11. The A_2 $\cos\theta$ decay distribution in the Gottfried-Jackson frame where the angle θ is the angle between the incoming π^- and the outgoing K^- in the A_2 rest frame. The solid line is the fit to the data explained in the text.

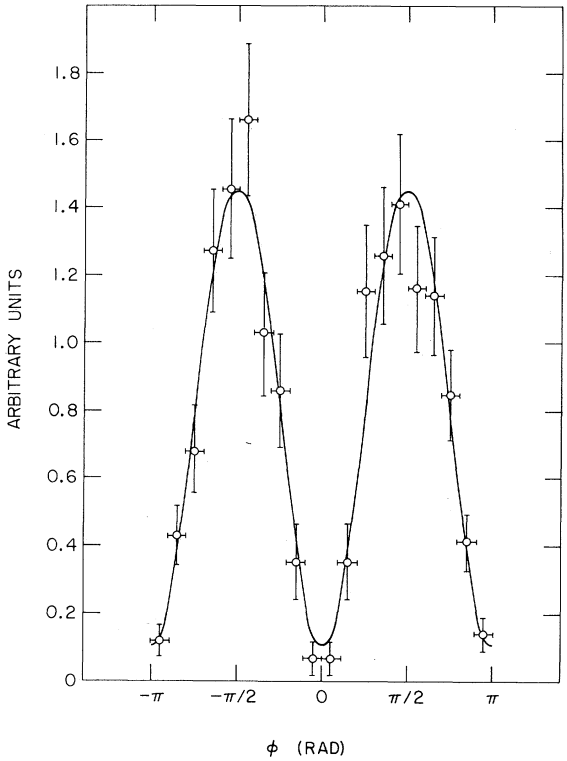

FIG. 12. The distribution of A_2 decays in the azimuthal angle ϕ. ϕ is the angle between the plane of production and the decay plane in the A_2 rest frame. The solid line is the fit to the data explained in the text.

The projected angular distribution in the Gottfried-Jackson frame is shown as a function of $\cos\theta$ and ϕ in Figs. 11 and 12. We have corrected the data for the acceptance of the apparatus. The large statistical errors for positive values of $\cos\theta$ reflect the low acceptance for low-momentum K^0's. The shape looks quite similar to the $\cos^2\theta \sin^2\theta \times \sin^2\phi$ distribution expected from ρ and f^0 exchange[12] (i.e., $\rho_{11} = \rho_{1\,-1} = \frac{1}{2}$). However, there is a slight deviation from this shape, so we have included ρ_{00}, ρ_{22}, $\rho_{2\,-2}$ in the fit. The fit was constrained by the physical requirements for the density matrix, i.e., $\rho_{00} + 2\rho_{11} + 2\rho_{22} = 1$, ρ_{00}, ρ_{11}, and ρ_{22} all real and positive, and $|\rho_{1\,-1}| \leq \rho_{11}$, $|\rho_{2\,-2}| \leq \rho_{22}$. A maximum-likelihood search was performed with the program MINUIT,[13] and the results are given in Table III for various regions of t'. The lines shown in Figs. 11 and 12 correspond to the fit in Table III for the range $0 \leq |t'| \leq 0.6$ $(\mathrm{GeV}/c)^2$. The errors on the parameters correspond to the variation required to reduce the natural log of the likelihood by $\frac{1}{2}$ (i.e., one standard deviation), and the notation "lim" in the table indicates where this could not be accomplished without violating the constraints on the parameters.

TABLE III. Results of a constrained maximum-likelihood fit to the first three terms of Eq. (1). Errors shown are standard deviations except where one standard deviation applied to a parameter would violate a constraint. This is indicated in the table by the notation "lim."

t' region $[(\mathrm{GeV}/c)^2]$	ρ_{00}	ρ_{11}	$\rho_{1\,-1}/\rho_{11}$	ρ_{22}	$\rho_{2\,-2}/\rho_{22}$	$\chi^2(\cos\theta)$ (17 d.f.)	$\chi^2(\phi)$ (7 d.f.)
0 to −0.1	$0.108^{+0.043}_{-0.037}$	$0.415^{+0.023}_{-0.026}$	$0.912^{+0.076}_{-0.086}$	$0.031^{+0.025}_{-0.023}$	$0.13^{+\mathrm{lim}}_{-1.10}$	21.7	1.8
−0.1 to −0.2	$0^{+0.011}_{-\mathrm{lim}}$	$0.486^{+\mathrm{lim}}_{-0.020}$	$0.949^{+\mathrm{lim}}_{-0.071}$	$0.014^{+0.020}_{-\mathrm{lim}}$	$1.0^{+\mathrm{lim}}_{-0.9}$	16.7	5.9
−0.2 to −0.6	$0^{+0.022}_{-\mathrm{lim}}$	$0.451^{+0.016}_{-0.019}$	$1.0^{+\mathrm{lim}}_{-0.013}$	$0.049^{+0.018}_{-0.016}$	$-1.0^{+0.8}_{-\mathrm{lim}}$	17.4	9.5
0 to −0.6	$0.046^{+0.019}_{-0.017}$	$0.451^{+0.011}_{-0.012}$	$0.948^{+0.035}_{-0.038}$	$0.026^{+0.012}_{-0.011}$	$-0.54^{+0.57}_{-\mathrm{lim}}$	26.5	6.2

TABLE IV. Results of a constrained maximum-likelihood fit to Eq. (1). The column labeled £ is the ratio of the likelihood obtained for this fit to that for the fits of Table III.

t' region [(GeV/c)^2]	ρ_{00}	ρ_{11}	Reρ_{10}	ρ_{1-1}	ρ_{22}	Reρ_{21}	Reρ_{20}	Reρ_{2-1}	ρ_{2-2}	$\chi^2(\cos\theta)$ (17 d.f.)	$\chi^2(\phi)$ (5 d.f.)	£
0 to −0.1	0.098	0.415	0.025	0.382	0.036	0.021	0.002	0.020	0.007	21.4	1.9	3.0
−0.1 to −0.2	0.008	0.491	−0.013	0.450	0.005	0	0	0	0.005	16.2	6.8	1.6
−0.2 to −0.6	0	0.450	0	0.450	0.050	−0.015	0	−0.015	−0.050	16.2	8.8	1.6
0 to −0.6	0.046	0.451	−0.001	0.427	0.026	−0.003	0	−0.003	−0.015	26.4	6.0	1.03

In each case, an acceptable χ^2 is obtained for both θ and ϕ distributions. Except perhaps at small $|t|$, ρ_{00} is small, indicating that exchange of particles with natural spin-parity dominates.

Finally, although the statistical accuracy is marginal, we have done a full density-matrix fit including all eight adjustable parameters. The fit was constrained by the limits imposed on the density matrix by the positivity conditions for an object of spin 2.[14] The results are given in Table IV. The column labeled £ gives the likelihood ratio for the eight-parameter fit versus the four-parameter fit given in Table III. Clearly, no significant improvement is obtained, and the new parameters are close to zero. This indicates that the density matrix elements in Table III are a good representation of the data.

V. RELATED EXPERIMENTS

Since the conclusion of this experiment, there have been reports on a number of other experiments which have examined the question of structure in the A_2 mass spectrum. The statistically most significant of these experiments[15] all report no evidence for structure.

Of the remaining experiments,[16] some claim evidence for structure; others claim evidence for no structure. Because of a lack of sufficient numbers of events in the A_2 mass region, or high backgrounds, or both, these experiments are unable to make statistically convincing arguments on the question of A_2 splitting.

VI. SUMMARY

This experiment has shown that in the K^0K^- decay channel, the A_2 meson has all the expected characteristics of a single resonance with quantum numbers $I=1$, $J^P=2^+$. A split structure of the type observed for this resonance in the CERN missing-mass spectrometer is ruled out for our mass spectrum (see Fig. 8). The decay angular distribution may be explained by a dominant exchange of natural spin-parity objects (ρ^0 and f^0) in the production process: The production t distribution shows a strong forward dip as expected for such processes.

VII. ACKNOWLEDGMENTS

We wish to thank the members of the AGS and EP & S Divisions of the Accelerator Department of Brookhaven National Laboratory for their help in the execution of this experiment. We thank our group technicians for their extended and valuable efforts in the construction and operation of the spectrometer. We acknowledge with thanks the aid and cooperation of the staff of the BNL On-Line Data Facility during the course of this experiment. We express our appreciation to Dr. David Cheng for his assistance with the programming in the early stages of this experiment.

*Work performed under the auspices of the U. S. Atomic Energy Commission.

[1]M. Alston-Garnjost, A. Barbaro-Galtieri, W. F. Buhl, S. E. Derenzo, L. D. Epperson, S. M. Flatté, J. H. Friedman, G. R. Lynch, R. L. Ott, S. D. Protopopescu, M. S. Rabin, and F. T. Solmitz, Phys. Letters 33B, 607 (1970).

[2]G. E. Chikovani, M. N. Focacci, W. Kienzle, C. Lechanoine, B. L. Levrat, B. Maglić, M. Martin, P. Schübelin, L. Dubal, M. Fischer, P. Grieder, H. A. Neal, and C. Nef, Phys. Letters 25B, 44 (1967); H. Benz, G. E. Chikovani, G. Damgaard, M. N. Focacci, W. Kienzle, C. Lechanoine, M. Martin, C. Nef, P. Schübelin, R. Baud, B. Bosnjakovic, J. Cotteron, R. Klanner, and A. Weitsch, *ibid.* 28B, 233 (1968); R. Baud, H. Benz, B. Bosnjakovic, D. R. Botterill, G. Damgaard, M. N. Focacci, W. Kienzle, R. Klanner, C. Lechanoine, M. Martin, C. Nef, V. Roinishvili, P. Schübelin, A. Weitsch, H. Blumenfeld, H. Jöstlein, and P. Lecomte, *ibid.* 31B, 397 (1970).

[3]Review of and references to such papers are contained in *Experimental Meson Spectroscopy*, edited by C. Baltay and A. H. Rosenfeld (Columbia Univ. Press, New York, 1970).

[4]S. U. Chung, O. I. Dahl, L. M. Hardy, R. I. Hess, G. R. Kalbfleisch, J. Kirz, D. H. Miller, and G. A. Smith, Phys. Rev. Letters 12, 621 (1964); D. J. Crennell, U. Karshon, K. W. Lai, J. M. Scarr, and I. O. Skillicorn, *ibid.* 20, 1318 (1968).

[5]K. J. Foley, W. A. Love, S. Ozaki, E. D. Platner, A. C. Saulys, E. H. Willen, and S. J. Lindenbaum, Phys. Rev. Letters 26, 413 (1971).

[6]K. J. Foley, W. A. Love, S. Ozaki, E. D. Platner, A. C. Saulys, E. H. Willen, and S. J. Lindenbaum (unpublished).

[7]K. Gottfried and J. D. Jackson, Nuovo Cimento 33, 309 (1964).

[8]J. D. Jackson, Nuovo Cimento 34, 1644 (1964).

[9]This shape is very close to the functional form suggested by Quigg and von Hippel (Ref. 3, p. 477):

$$\Gamma(m) = \Gamma_0 \frac{\rho(q)}{\rho(q_0)} ,$$

where

$$\rho(q) = \frac{qR}{|H_2^{(1)}(qR)|^2} .$$

$H_2^{(1)}$ is the Hankel function of the first kind.

[10]A more refined Monte Carlo calculation of the acceptance has modified these numbers slightly from those published earlier (Ref. 5).

[11]In order to estimate the possible size of background, we have fitted the data over the mass region 1.1–1.5 GeV allowing a linear background term. After correction for the acceptance, a background level of 1.6 ± 0.7 events/bin was found, while the peak height is ≈30 events/bin.

[12]J. L. Rosner, in *Phenomenology in Particle Physics*, edited by C. B. Chiu, G. C. Fox, and A. J. G. Hey, (Caltech, Pasadena, 1971).

[13]F. James and M. Roos, CERN Computer Program Library Reports No. D506 and No. D516 (unpublished).

[14]R. H. Dalitz, Nucl. Phys. 87, 89 (1966); S. U. Chung (unpublished).

[15]G. Grayer, B. Hyams, C. Jones, P. Schlein, W. Blum, H. Dietl, W. Koch, H. Lippmann, E. Lorenz, G. Lütjens, W. Männer, J. Meissburger, U. Stierlin, and P. Weilhammer, Phys. Letters 34, B333 (1971); D. Bowen, D. Earles, W. Faissler, D. Garelick, M. Gettner, M. Glaubman, B. Gottschalk, G. Lutz, J. Moromisato, E. I. Shibata, Y. W. Tang, E. von Goeler, H. R. Blieden, G. Finocchiaro, J. Kirz, and R. Thun, Phys. Rev. Letters 26, 1663 (1971); D. Underwood, G. Conforto, M. A. Kramer, R. Prepost, D. H. Tompkins, M. S. Witherell, A. W. Key, and R. M. Mobley, Bull. Am. Phys. Soc. 17, 64 (1972) and private communication with M. A. Kramer; D. M. Binnie, L. Camilleri, A. Duane, A. R. Faruqi, D. A. Garbutt, W. G. Jones, M. E. Kay, M. Lewis, P. J. Nicholson, I. Siotis, P. N. Upadhyay, J. G. Wilson, I. F. Burton, S. G. Frank, R. George, M. Haque, and J. G. McEwen, Phys. Letters 36B, 257 (1971).

[16]M. Basile, P. Dalpiaz, P. L. Frabetti, T. Massam, F. Navach, F. L. Navarria, M. A. Schneegans, and A. Zichichi, Lett. Nuovo Cimento 4, 838 (1970); K. W. J. Barnham, G. S. Abrams, W. R. Butler, D. G. Coyne, G. Goldhaber, B. H. Hall, J. MacNaughton, and G. H. Trilling, Phys. Rev. Letters 26, 1494 (1971); D. J. Crennell, H. A. Gordon, K. W. Lai, and J. M. Scarr, Phys. Letters 35B, 185 (1971); D. M. Binnie, L. Camilleri, A. Duane, D. A. Garbutt, J. R. Holmes, W. H. Jones, J. Keyne, M. Lewis, I. Siotis, P. N. Upadhyay, I. F. Burton, R. George, and J. G. McEwen, *ibid.* 36B, 537 (1971); I. J. Bloodworth, W. C. Jackson, J. D. Prentice, and T. S. Yoon, Nucl. Phys. B37, 203 (1972).

PHYSICAL REVIEW D VOLUME 6, NUMBER 3 1 AUGUST 1972

Measurement of the Differential Cross Section for $\pi^- p \to n\pi^0$ at 317, 452, and 491 MeV/c*

P. A. Berardo,† R. P. Haddock, B. M. K. Nefkens, L. J. Verhey,‡ and M. E. Zeller§
University of California, Los Angeles, California 90024

and

A. S. L. Parsons‖ and P. Truoel**
Lawrence Berkeley Laboratory, University of California, Berkeley, California 94720
(Received 27 March 1972)

Seventeen differential cross sections of the pion-nucleon charge-exchange reaction have been measured at total center-of-mass energies of 1245, 1337, and 1363 MeV. Most measurements are based on the neutron-photon coincidence method, using carefully calibrated neutron counters and an efficient, large-area photon detector. The results are used to test the predictions of charge independence, with which they agree. The results also confirm the Ayed-Bareyre-Sonderegger phase-degeneracy hypothesis at $\tilde{\theta}_{\pi^0} = 180°$.

I. INTRODUCTION

We have measured the differential cross sections for the pion-nucleon charge-exchange (CEX) reaction,

$$\pi^- p \to \pi^0 n ,$$

at 317-, 452-, and 491-MeV/c pion momenta in the laboratory, corresponding to $\tilde{E} = 1245$-, 1337-, and 1363-MeV center-of-mass total energies.